Ionic Interactions in Crystalline Bovine Pancreatic Ribonuclease A[†,‡]

Alexander A. Fedorov,[§] Diane Joseph-McCarthy,[||] Elena Fedorov,[§] Dora Sirakova,[§] Isaac Graf,[§,⊥] and Steven C. Almo*[,§]

Department of Biochemistry, Albert Einstein College of Medicine, 1300 Morris Park Avenue, Bronx, New York 10461, and Department of Biological Chemistry and Molecular Pharmacology, Harvard Medical School, Boston, Massachusetts 02115

Received June 25, 1996; Revised Manuscript Received September 17, 1996[⊗]

ABSTRACT: Isomorphous crystals (space group $P3_221$) of bovine pancreatic ribonuclease A (RNase A) were prepared at a pH of 5.5 in a series of high salt conditions, where both the nature of the ions and the ionic strength varied: 80% ammonium sulfate ($\mu = 12.5$); 8 M sodium formate ($\mu = 8.0$); 3 M NaCl, 30% ammonium sulfate ($\mu = 7.0$); 3 M CsCl, 30% ammonium sulfate ($\mu = 7.0$); and 2.5 M NaCl, 3.3 M sodium formate ($\mu = 5.8$). These structures were independently refined to a resolution of 2.0 Å or better with *R*-factors that range from 16.1% to 17.5%. A comparison of these six structures and the monoclinic crystal form of RNase A grown from alcohol shows that changes in ionic strength do not alter the secondary or tertiary sturcture and that there are no significant changes in intramolecular salt bridges. These findings support the notion that structures determined from crystals grown in high salt are representative of the overall structural and electrostatic features present under physiological conditions. While little effect was observed on the main chain conformation, several residues adopted different side chain conformations and altered hydrogen-bonding patterns, either as result of direct anion binding or more subtle indirect effects. Changes in the ionic composition of the mother liquor allowed for the occupancy of the active site with different anions. The direct observation of active site-bound chloride and formate anions supports the proposal that these species act as true competitive inhibitors of RNase A and not through nonspecific electrostatic effects. The identification of bound formate anions allowed for an experimental validation of computational-based functional group mapping techniques and suggests a useful modification to these approaches. Electrostatic surface potential calculations identify a nearly continuous band of positive potential, consistent with an extended binding site for polynucleotide ligands and substrates. The majority of these residues are not involved in salt bridges, which may facilitate binding to extended polynucleotide substrates. Selection of the appropriate solvent conditions results in an unoccupied active site, which will allow this crystal form to be used for the crystallographic study of productive ligand-binding modes.

Bovine pancreatic ribonuclease (RNase A)[1] is a cornerstone of protein structure and function. RNase A was the first protein to have its amino acid sequence determined (124 amino acids) (Pott et al., 1962; Smyth et al., 1963) and one of the first proteins to yield an X-ray structure (Kartha et al., 1967). RNase A is the archetype of the RNase superfamily, a family of homologous proteins sharing greater than 30% sequence identity, which are found in nearly all fluids and tissues of mammals and in some reptiles (Bientema et al., 1988). These proteins are highly specific for catalyzing the hydrolysis (transphosphorylation) of single-stranded ribonucleic acid (RNA) at pyrimidine residues to yield 2′,3′-cyclic pyrimidine phosphates and a free 5′-hydroxyl. Individual members of the superfamily catalyze this reaction at very different rates, with k_{cat}/K_m spanning over 6 orders of magnitude (Lee & Vallee, 1989). RNase A and the more active members of this superfamily also catalyze the hydrolysis of the 2′,3′-cyclic phosphate to specifically yield the 3′-pyrimidine monophosphate. Despite the large kinetic differences, the entire superfamily is thought to utilize a common mechanism, as the residues considered essential for substrate binding and catalysis (i.e., His-12, Lys-41, Thr-45, and His-119) are strictly conserved.

Kinetics, chemical modification (Richardson et al., 1990; de Llorens et al., 1989; Pares et al., 1980), NMR (Haffner & Wang, 1973; Gorenstein & Wyrwicz, 1973; Meadows et al., 1969), crystallographic (Richards & Wyckoff, 1971), and site directed mutagenesis (Tarragona-Fiol et al., 1993; delCardayre & Raines, 1994) studies have provided details about the enzymatic mechanism and have lead to models of mononucleotide, dinucleotide, and extended ligand binding (see Figure 1). The enzyme-catalyzed reaction proceeds through a trigonal-bipyramidal transition state, with inversion of configuration around the phosphorus center (Usher et al., 1970, 1972). Although other mechanisms have been proposed (Witzel, 1963; Ruterjans & Witzel, 1969), the enzyme is generally thought to utilize an in-line mechanism in which

[†] This work is supported by Grant GM50121 (S.C.A.) from the National Institutes of Health and an award from the W. M. Keck Foundation.

[‡] Coordinates for these structures have been deposited with the Brookhaven Protein Data Bank (PDB filenames: 1RNO, 1RNQ, 1RNW, 1RNX, 1RNY, and 1RNZ).

* Please address correspondence to this author at Albert Einstein College of Medicine. Phone: (718) 430-2746. FAX: (718) 430-8565. E-mail: almo@zugbug.bioc.aecom.yu.edu.

[§] Albert Einstein College of Medicine.

[||] Harvard Medical School.

[⊥] Present address: Department of Electrical Engineering and Computer Science, Massachusetts Institute of Technology, Cambridge, MA 02139.

[⊗] Abstract published in *Advance ACS Abstracts,* November 15, 1996.

[1] Abbreviations: RNase A, bovine pancreatic ribonuclease A; μ, ionic strength.

S0006-2960(96)01533-4 CCC: $12.00

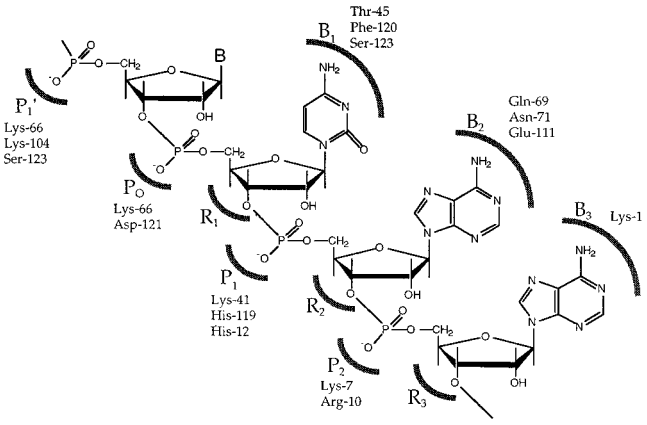

FIGURE 1: Schematic of the proposed subsites for the binding of extended ligands by RNase A.

His-12 and His-119 act alternately as general acids/bases during catalysis, with Lys-41 providing some degree of electrostatic stabilization to the transition state. The specificity for pyrimidines arises primarily from specific hydrogen bonds formed between the base and the backbone amide NH and the side chain hydroxyl of Thr-45. His-119 displays substantial conformational flexibility which may be important to catalysis. In several different crystals structures, the His-119 side chain occupies two major conformations that have been denoted A and B by Borkakoti (1982, 1983) and are related by approximately a 180° torsion about the $C_\alpha-C_\beta$ bond.

The modulation of solvent conditions, such as ionic strength and ionic composition, can have significant effects on the activity of an enzyme. Enunciating such correlations is fundamental to understanding the determinants of enzymatic catalysis and specificity and is expected to be particularly important in the case of enzymes such as ribonuclease which act on polyanionic substrates. The utilization of X-ray crystallography to identify alterations in the native enzyme, or the solvent structure, in response to ionic conditions may indicate properties important for catalysis, such as active site flexibility. Furthermore, the direct observation of anion-binding sites can establish modes of inhibition and reveal anion subsites which are occupied by extended polyanionic ligands. Additionally, this approach offers the opportunity for experimental verification of computational methods directed at predicting functional group binding sites.

Considerable crystallographic work has been performed on monoclinic crystals ($P2_1$) grown from alcohols (Campbell & Petsko, 1987, Borkakoti et al., 1982; Borkakoti, 1983; Wlodadwer et al., 1988), trigonal crystals ($P3_121$) of RNase S, the noncovalent complex formed by subtilisin cleavage of RNase A (1−20:21−124) (Richards & Wyckoff, 1973), and ligand complexes of these forms (Richards & Wyckoff, 1973; Wodak et al., 1977; Pavlovsky et al., 1978; Borah et al., 1985; Aguilar et al., 1991, 1992). An unrelated trigonal form ($P3_221$, referred to as form W) of another noncovalent complex composed of residues 1−118 and 111−124 has also received considerable attention (Martin et al., 1987). Both noncovalent analogs have allowed for the production and study of semisynthetic mutants of ribonuclease (deMel et al., 1991, 1994; Varadarajan & Richards, 1992). These semisynthetic systems are limited because they only allow for alterations near the amino and carboxy termini. A complete understanding of RNase A function requires the crystallographic examination of general mutants produced by site-directed mutagensis. Form W crystals are particularly attractive for the study of enzyme−ligand complexes as the active site is located in a large solvent-filled channel and the high symmetry allows for efficient data collection. The success of structural work on RNase A−ligand complexes, however, requires the removal of the inhibitory sulfate/phosphate from the active site (Campbell & Petsko, 1987; Wlodawer et al., 1988). This is a particular challenge in the case of form W crystals, which are grown from concentrated solutions of ammonium sulfate.

We report the refined structures of full-length native RNase A from form W crystals in a series of ionic conditions. This includes the first report of a recombinant RNase A structure. These structures show that the side chain conformation of several residues, including some involved in substrate binding and catalysis, is responsive to ionic conditions, either through direct binding of ions or through indirect solvent effects. These results show that anion binding in the active site can be readily manipulated. Conditions to obtain form W crystals with inhibitor-free active sites are determined and provide the information needed to fully exploit this crystal form for the study of RNase A−ligand complexes.

MATERIALS AND METHODS

Preparation of Recombinant RNase A. Bona fide full-length RNase A used for preparation of the W1, W3, W4, W5, and W6 crystal forms (Table 1) was from Sigma. Recombinant RNase A (W2) was prepared by the method of Laity et al. (1993). RNase A was expressed as a fusion protein with the gene 10 protein under control of an IPTG-inducible T7 promoter in the *Escherichia coli* strain HMS174-(DE3)-pLys(S). Protein isolation, factor Xa digestion, purification, folding, and activity measurements were performed, as described (Laity et al., 1993).

Crystallization. Crystallization and soaking conditions for the RNase A (form W) crystals used in this work are summarized in Table 1. All crystals were grown by hanging drop vapor diffusion using 5 μL of protein (50 mg/mL) mixed with 5 μL of precipitant suspended over a 1 mL reservoir. All crystals had dimensions of ~0.25−1 mm^3. Crystals of bona fide (W1) and recombinant (W2) RNase A were grown from ~30% ammonium sulfate, 3.0 M CsCl, and 0.1 M sodium acetate, pH 5.5, at room temperature. Prior to data collection these crystals were soaked for 1−3 h in 80% saturated ammonium sulfate and 0.1 M sodium acetate, pH 5.5, to remove the Cs^+ cations which diminish the effective resolution due to absorption effects. Crystals grown under the above conditions and used without removal of CsCl are designated W3. Crystals grown from 30% saturated ammonium sulfate, 3.0 M NaCl, and 0.1 M sodium acetate, pH 5.5 (W4), were mounted directly without soaking. These conditions (W4) are similar to those described for crystallization of a fluorescent derivative of RNase A (Bandet-Nassler et al., 1993). Form W5 crystals were obtained from 3 M sodium formate, 3 M CsCl, and 0.1 M sodium acetate, pH 5.5, and the CsCl was washed out with a stabilizing buffer composed of 8 M sodium formate and 0.1 M sodium acetate, pH 5.5. Form W6 crystals were obtained from 3.3 M sodium formate, 2.5 M NaCl, and 0.1 M sodium acetate, pH 5.5. These crystals exhibit the symmetry of space group $P3_221$

Table 1: Crystallization and Data Collection Conditions for RNase A (W Form) Crystals

code	crystallization conditions	data collection conditions	μ^a	unit cell[b] (Å)
W1	3 M CsCl, 30% $(NH_4)_2SO_4$, 0.1 M CH_3COONa, pH 5.5	80% $(NH_4)_2SO_4$, 0.1 M CH_3COONa, pH 5.5	12.5	$a = 65.10$, $c = 65.52$
W2[c]	same as for W1	same as for W1	12.5	$a = 64.61$, $c = 65.19$
W3	3 M CsCl, 30% $(NH_4)_2SO_4$, 0.1 M CH_3COONa, pH 5.5	same as crystallization	7.0	$a = 64.76$. $c = 65.34$
W4	3 M NaCl, 30% $(NH_4)_2SO_4$, 0.1 M CH_3COONa, pH 5.5	same as crystallization	7.0	$a = 64.66$, $c = 65.25$
W5	3 M CsCl, 3 M COONa, 0.1 M CH_3COONa, pH 5.5	8 M COONa, 0.1 M CH_3COONa, pH 5.5	8.0	$a = 64.94$, $c = 65.29$
W6	2.5 M NaCl, 3.3 M COONa, 0.1 M CH_3COONa, pH 5.5	same as crystallization	5.8	$a = 64.56$, $c = 65.15$

[a] Ionic strength; $\mu = \sum cz^2/2$. [b] All crystals exhibit symmetry consistent with space group $P3_221$ and have one molecule per asymmetric unit. [c] Recombinant RNase A.

Table 2: Summary of Data and Refinement of RNase A (W Form) Crystals

	W1	W2	W3	W4	W5	W6
Data Collection						
resolution (Å)	1.9	1.8	2.0	1.9	2.0	1.9
unique reflections	12384	13874	9388	10518	9461	11350
merging *R*-factor (%)	4.1	3.4	4.4	3.5	3.6	4.9
completeness (%)	94.9	92.6	84.5	82.7	86.8	89.0
Refinement						
resolution range (Å)	8−1.9	8−1.8	8−2.0	8−1.9	8−2.0	8−1.9
R-factor (%)	16.5	16.7	17.5	16.2	16.1	16.7
reflections used	12047	12877	8896	9960	8832	10380
no. of waters	112	110	99	103	89	95
no. of ions	$2SO_4^{2-}$	$2SO_4^{2-}$	$4Cl^-$, $1Cs^+$	$4Cl^-$	$2COO^-$	$3Cl^-$
mean *B*-factor	27.4	23.2	17.4	19.4	25.7	22.9
main chain	25.7	21.5	15.8	17.7	24.0	21.4
side chain	29.3	25.1	19.2	21.3	27.6	24.6
waters	48.7	42.5	28.5	37.2	42.8	38.8
Stereochemistry (RMS Deviation from Target)						
distances (Å)						
bond lengths	0.015	0.011	0.011	0.011	0.012	0.011
angles 1−3	0.038	0.030	0.032	0.029	0.033	0.030
planar 1−4	0.043	0.038	0.039	0.040	0.041	0.039
planes	0.014	0.011	0.012	0.011	0.011	0.011
chiral volumes (Å^3)	0.158	0.136	0.140	0.120	0.142	0.114
nonbonded (Å)						
single torsion	0.166	0.172	0.174	0.171	0.168	0.172
multiple torsion	0.188	0.176	0.201	0.181	0.191	0.198
H-bond	0.224	0.204	0.200	0.215	0.195	0.236
torsion angles (deg)						
planar	2.4	1.8	1.9	1.7	1.7	1.6
staggered	16.7	15.9	15.4	16.0	17.3	17.0
orthonormal	19.6	19.9	18.3	18.4	21.6	17.6
B-factors (Å^2)						
main chain 1−2	1.51	1.38	1.61	1.36	1.34	1.32
main chain 1−3	2.49	2.35	2.63	2.34	2.33	2.29
side chain 1−2	3.07	2.71	2.90	2.61	2.70	2.48
side chain 1−3	4.90	4.37	4.43	4.22	4.31	3.95

with one molecule per asymmetric unit and diffract to greater than 2.0 Å resolution.

Data Collection and Processing. All data were collected at room temperature with a Siemens multiwire area detector coupled to a Rigaku RU-200 rotating anode generator operating in fine focus mode (50 kV, 80 mA, $\lambda = 1.5418$ Å). A single crystal was used for each data set, and the data were reduced with XDS (Kabsch, 1988) (see Table 2 for data collection statistics).

Refinement. The starting model used for the refinement of W1 (80% saturated ammonium sulfate) was the semisynthetic RNase (1−118:111−124) described in file 1SRN (Martin et al., 1987) of the Protein Data Bank (Bernstein et al., 1977), excluding ordered solvent molecules and sulfate ions. The W1 crystals ($a = b = 65.10$ Å and $c = 65.52$ Å) were not completely isomorphous with the starting model ($a = b = 67.68$ Å and $c = 65.01$ Å). Rigid body refinement was applied in successive resolution ranges (10−5, 10−4, 10−3 Å) to adjust the orientation of the model, resulting in an *R*-factor of 34.2% in the 10−3 Å resolution shell. Several rounds of simulated annealing with X-PLOR (Brünger et al., 1987; Brünger, 1992), followed by manual intervention using $2F_o - F_c$ and $F_o - F_c$ maps, were carried out to improve the model. Major rebuilding was required in the region 112−115, as the semisynthetic starting model is composed of two fragments which lack covalent continuity in this region. Water molecules and ions were added at stereochemically reasonable positions with significant density in difference Fouriers ($>3\sigma$). In evaluating hydrogen bonds, a distance criterion of 2.4−3.6 Å and a cutoff value of 110° for the donor atom−hydrogen atom−acceptor atom angle were used. All waters were assigned unit occupancy, and individual atomic *B*-factors were refined for all non-hydrogen atoms. Refinement was completed with X-PLOR and conventional least squares refinement (Hendrickson, 1985), using PROFFT (Finzel, 1987), the fast Fourier version of PROLSQ (Hendrickson, 1985) which incorporates intermolecular restraints (Sheriff, 1987). Refinement for the W1

structure converged with an *R*-factor of 0.165 for the 12 047 reflections with $F > 2\sigma(F)$ in the 8.0−1.9 Å resolution range. All remaining structures, W2, W3, W4, W5, and W6 (Tables 1 and 2), were refined with the same protocol described above using the final W1 structure, excluding waters and ions, as the starting model. Due to the resolution of this work, 1.8−2.0 Å, alternate side chain conformations were not modeled.

All potential ions were initially modeled as waters. The identification of a particular feature as an ion was based on careful examination of residual electron density in difference Fouriers and the refined occupancies and *B*-factors. All anions (i.e., sulfate, formate, and chloride) refined with occupancies very close to unity and full occupancy was assumed (Table 2). The occupancy of the Cs^+ cation in W3 was refined to a value of 0.32. All ions were confirmed with simulated annealing omit maps.

Electrostatic Surface Potential Calculations. The refined coordinates of RNase A (W6) were used to calculate the electrostatic potential surface with DELPHI (Nicholls et al., 1991). Dielectric constants of 2 and 80 were employed for the solvent and protein, respectively. Histidine residues were modeled with a charge of +0.5.

Functional Group Maps. The multiple copy simultaneous search (MCSS) algorithm (Miranker & Karplus, 1991) is expected to predict the preferred binding sites for a given functional group in or on a known macromolecular structure. Functional group maps of formate were calculated for the W5 RNase A structure using MCSS. For each MCSS calculation, 2000 copies of the functional group were randomly distributed in a 15 Å radius sphere (centered on His-12 ND1) that includes most of the RNase A structure. The group copies were then simultaneously energy minimized in the full force field of the fixed protein (the group copies do not interact with each other). All of the energy and minimization calculations were performed with CHARMM (Brooks et al., 1983) version 22 and the standard PARAM19 (polar hydrogen parameters and topologies). An 8 Å cutoff on nonbonded energy terms (achieved via a shift truncation function) and a dielectric constant of unity were employed throughout. The formate functional group was modeled as an extended atom carbon bonded to two equivalent oxygen atoms with an overall net charge of −1. Calculations were performed with hisidines either singly protonated on ND1 (net charge of 0) or doubly protonated (net charge of +1). A detailed description of the calculations is reported elsewhere (Joseph-McCarthy et al., 1996).

RESULTS

Quality of the Models. The *R*-factors for these structures range from 16.1% to 17.5%, and all possess good stereochemistry (0.011−0.017 Å RMS bond lengths, 2.39−3.08° RMS bond angles). A summary of the refinement statistics is presented in Table 2. All models contain 951 non-hydrogen protein atoms, with the exception of W1 (80% saturated ammonium sulfate) which has 944 atoms due to poor electron density of the amino-terminal lysine, and all have approximately 100 water molecules. The final models for the bona fide RNase A (W1) and recombinant RNase A (W2) in 80% ammonium sulfate both contain two bound sulfate anions. Form W3 (30% saturated ammonium sulfate, 3 M CsCl) contains four chloride anions with an occupancy of 1.0 and a single cesium cation with a refined occupancy of 0.32. The final model for W4 (30% ammonium sulfate, 3 M NaCl) contains four chloride anions with an occupancy of 1.0 and no bound sulfate anions. The final model for W5 (8 M formate) contains two formate anions bound in the active site. Form W6 (2.5 M NaCl, 3.3 M sodium formate) contains three bound chlorides.

Table 3: Root-Mean-Square Differences (Å) between Six Structures of Trigonal RNase A (W Form) and Monoclinic RNase A (7RSA)[a]

structure	W1	W2	W3	W4	W5	W6	7RSA
W1	−	0.184	0.236	0.202	0.169	0.239	0.410
		0.184	0.253	0.229	0.171	0.248	0.421
W2	0.551	−	0.184	0.144	0.223	0.160	0.394
			0.201	0.168	0.241	0.195	0.432
W3	0.746	0.562	−	0.126	0.286	0.206	0.423
				0.132	0.333	0.186	0.456
W4	0.733	0.595	0.524	−	0.225	0.124	0.402
					0.279	0.109	0.441
W5	0.665	0.569	0.602	0.664	−	0.214	0.450
						0.280	0.479
W6	0.740	0.585	0.546	0.444	0.606	−	0.408
							0.446
7RSA	0.915	0.964	0.962	0.974	0.941	0.994	−

[a] The numbers in the upper triangular part of the matrix correspond to the RMS differences (Å) for 124 α-carbons and 495 main chain atoms. The lower left tiangular part of the matrix gives the RMS differences for all 951 atoms.

All non-glycine residues in the refined structures lie within "allowed" regions of the Ramachandran plot, except Gln-60, which adopts the same unusual conformation observed in the monoclinic crystals of native RNase A grown from alcohol (Wlodawer et al., 1982). The average temperature factors for side chain, main chain, and all protein atoms range from 19.2 to 29.3, 15.8 to 25.7, and 17.4 to 27.4 $Å^2$, respectively. The average temperature factors for water molecules are 48.7, 42.5, 28.5, 37.2, 42.8, and 38.8 Å for models W1, W2, W3, W4, W5, and W6, respectively. Despite the absolute differences in temperature factors between the individual structures, each of the six crystal forms shows very similar trends in the relative *B*-factors along the polypeptide chain.

On the basis of a Luzzati analysis (Luzzati, 1952), the upper limit of the mean coordinate error is estimated to be about 0.19 Å in all six structures reported here. Another estimate for the accuracy of the coordinates can be derived from a comparison of independently refined structures. The RMS deviation between pairs of structures for main chain atoms ranges from 0.13 to 0.33 Å (Table 3). The closest agreement (0.13 Å RMS deviation) is between W3 and W4, which both contain 30% ammonium sulfate and differ only in the counterion for chloride (i.e., cesium vs sodium). The most disparate structures are W3 and W5. The bona fide (W1) RNase A and recombinant (W2) RNase A have an RMS deviation of 0.18 Å (Table 3).

In all six structures, the first residue (Lys-1) is not clearly seen in the density due to disorder. The segments with the largest thermal parameters in all six structures correspond to five external loops (17−22, 35−40, 66−70, 87−95, and 112−114). Several side chains, all located in these surface loops, are poorly defined and have high thermal parameters ($B > 50$ $Å^2$). These include Ser-21, Lys-37, Asp-38, Arg-39, Gln-69, Ser-89, Lys-91, Tyr-92, Asn-94, and Asn-113 in all six models.

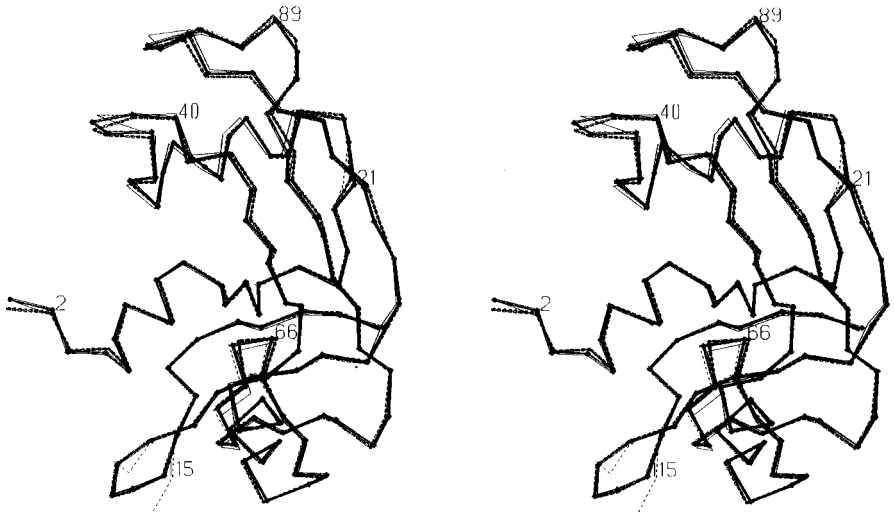

FIGURE 2: C_α trace of various RNase A structures in stereo: form W1 (heavy solid line), 7RSA (heavy dashed line), 1RNU (light solid line), and 1SRN (light dashed line).

Structure of RNase A in Trigonal Form W and Comparison with Monoclinic RNase A Structure. The overall structure of RNase A is very similar in all crystal forms studied. The α-carbon traces of trigonal native RNase A (W1), the 1.26 Å resolution monoclinic native RNase A structure from alcohol (7RSA), the semisynthetic $P3_121$ RNase S (1RNU), and the semisynthetic trigonal $P3_221$ RNase A (1SRN) are shown in Figure 2. The greatest similarity in this group is observed between the two W form structures, native trigonal RNase A (W1) and the starting model for our refinement, semisynthetic trigonal RNase A (1SRN), both of which are prepared from 80% saturated ammonium sulfate (RMS = 0.27 Å, excluding the segment 112−115). The largest difference between these two structures occurs in the chain segment 112−115 due to the covalent discontinuity in the semisynthetic structure (RMS = 0.46 Å when all α-carbons are considered).

The six structures of refined trigonal native RNase A and the 1.26 Å structure of monoclinic RNase A have been compared by a least squares fitting algorithm (Rossmann & Argos, 1975) (see Table 3). All six models of trigonal native RNase A are very similar with maximal pairwise RMS deviations of 0.28 and 0.33 Å for C_α alone and for all main chain atoms, respectively (Table 3). Several side chains in regions with high temperature factors have RMS deviations greater than 1 Å. The electrostatic interactions, as enumerated by intramolecular salt bridges, are highly conserved in the seven RNase A structures.

In the trigonal crystal forms, four residues with well-defined electron density have distinctly different side chain conformations about χ_1 (Table 4). The side chains of Ser-77 and His-119 have one predominant conformation in models with highest ionic strength (W1 and W2) and a different conformation in models with lower ionic strength (W3−W6). The side chains of Thr-17 and Val-124 have one predominant conformation (A) in crystals containing 8 M sodium formate (model W5) and a second conformation (B) in all remaining models.

Conformation A (Table 4) of Thr-17 places OG1 of the side chain within hydrogen-bonding distance of His-48 ND1. In conformation B, which is produced by ∼90° rotation about the $C_\alpha-C_\beta$ bond, this hydrogen bond is absent and instead OG1 of Thr-17 forms a hydrogen bond to a water molecule.

Table 4: Side Chains Having Different Conformations in Different Salt Forms of Native Trigonal RNase A

			torsion angles (deg)		
residue	salt form	*B*-factor (Å^2)	χ_1	χ_2	conformation
Thr-17	w1	31.9	56		A
	w2	30.3	53		A
	w3	20.4	62		A
	w4	27.3	59		A
	w5	34.2	−18		B
	w6	33.6	71		A
Ser-77	w1	31.3	−144		B
	w2	22.9	−148		B
	w3	16.3	67		A
	w4	17.8	64		A
	w5	23.7	71		A
	w6	22.0	66		A
His-119	w1	32.6	−57	−70	B
	w2	32.7	−61	−64	B
	w3	25.3	159	69	A
	w4	31.0	150	77	A
	w5	30.3	159	72	A
	w6	29.9	152	79	A
Val-124	w1	31.6	−133		A
	w2	25.7	−162		A
	w3	18.9	−160		A
	w4	20.4	−167		A
	w5	28.6	40		B
	w6	25.2	−159		A

In both conformations, the side chains of Thr-17 and Asp-14 share a hydrogen bond. In conformation B, Ser-77 OG1 appears to be hydrogen bonded to Asn-34 ND2 of a symmetry-related molecule. In conformation A, this interaction is absent and Ser-77 is hydrogen bonded to the three neighboring water molecules. A hydrogen bond between Ser-77 OG1 and Ser-32 carbonyl oxygen of a symmetry-related molecule is found in both conformations. The two conformations of Val-124 differ by a 160° rotation of the isopropyl side chain. The RMS shift of this side chain in model W5 is 1.65 Å from its position in the other models.

Eleven residues with well-defined density in native trigonal RNase A (W1) have atomic positions with RMS side chain deviations from native monoclinic RNase A (7RSA) greater than 1.0 Å (see Table 5). Large deviations for the side chain positions of Glu-9, Ser-18, Lys-61, Gln-74, Ser-77, Arg-85, Lys-104, and Val-124 result from different intermolecular

Table 5: Side Chains Having Distinctly Different Conformations in Native Trigonal (W1) and Monoclinic (7RSA) RNase A[a]

residue	structure	torsion angles (deg) χ_1	χ_2	χ_3	χ_4	rms distance (Å) of side chain atoms	intermolecular contact[b]
Glu-9	W1	−73	168	−7			+
	7RSA	−61	−178	29		1.11	+
Ser-18	W1	81					−
	7RSA	−70				1.63	+
Lys-61	W1	−174	65	171	179		+
	7RSA (A)	−169	171	−152	164	1.60	+
	7RSA (B)	−176	65	−179	177	0.97	+
Asn-67	W1	70	7				−
	7RSA (A)	79	−21			0.84	−
	7RSA (B)	−70	−20			4.15	−
Gln-74	W1	−180	172	139			+
	7RSA	−177	−171	−54		1.62	−
Ser-77	W1	−144					+
	7RSA (A)	−70				1.27	−
	7RSA (B)	−29				1.75	−
Arg-85	W1	−172	148	−70	−114		+
	7RSA (A)	−149	94	59	−169	2.52	−
	7RSA (B)	143	−82	150	77	5.62	−
Gln-101	W1	168	67	29			−
	7RSA	−53	175	−31		3.99	−
Lys-104	W1	−59	−164	−49	137		+
	7RSA (A)	−74	−171	172	−64	2.04	−
	7RSA (B)	−49	−83	−166	78	1.51	−
His-119	W1	−57	−71				−
	7RSA	159	82			3.81	−
Val-124	W1	−134					+
	7RSA	−65				1.20	+

[a] All of this side chains are well defined in trigonal RNase A structures. [b] Hydrogen bonds less than 3.5 Å in length.

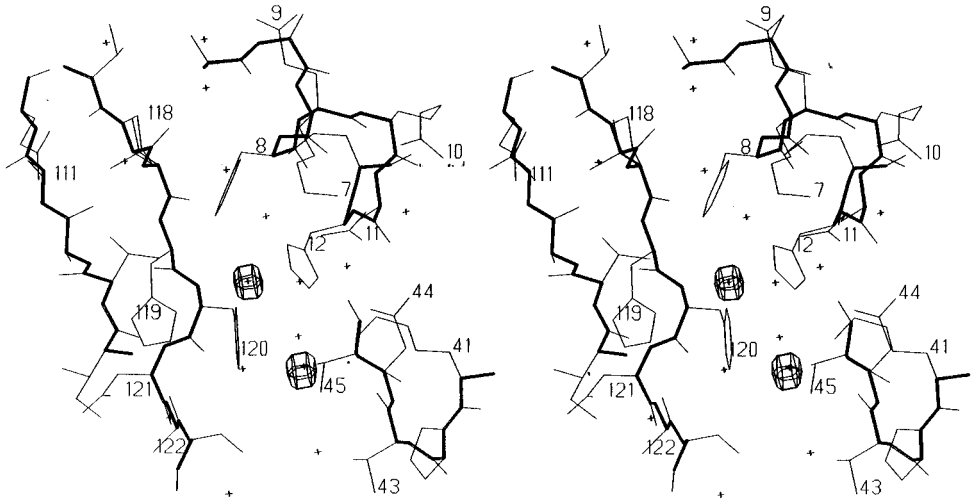

FIGURE 3: Stereoscopic view of the trigonal RNase A (W3) active site with two chloride ions bound.

contacts in the trigonal and monoclinic crystal forms (Table 5). Asn-67, Gln-101, and His-119 do not participate in intermolecular contacts in either crystal form. Gly-88 and Ser-89, which are not well defined in electron density, are the only residues whose main chain atoms in all six trigonal RNase A structures deviate by more than 1.0 Å from their positions in monoclinic RNase A.

Active Site. The most significant differences in the active sites of the six trigonal RNase A crystal forms are associated with differential ion binding (Figures 3−5). Crystals in 30% ammonium sulfate and either 3 M cesium chloride (W3) or 3 M sodium chloride (W4) each show two chloride ions bound in the active site with similar coordination patterns. These chloride ions were initially modeled as water but refined to very low temperature factors, and difference Fourier syntheses showed residual electron density. Modeling these features as chloride ions with unit occupancy, the temperature factors refined to 34.2 and 27.5 Å^2 for model W3 and 29.9 and 23.1 Å^2 for model W4, implying that these anion sites are highly occupied. Difference Fouriers based on the chloride model showed no residual density at these sites. The first chloride ion (CL-125), bound in the P_1 subsite, forms hydrogen bonds to atom NE2 of His-12 and the backbone amide of Phe-120 (Figure 3). CL-125 also forms hydrogen bonds to the two water molecules (WAT-232 and WAT-279; W4 numbering). The second chloride

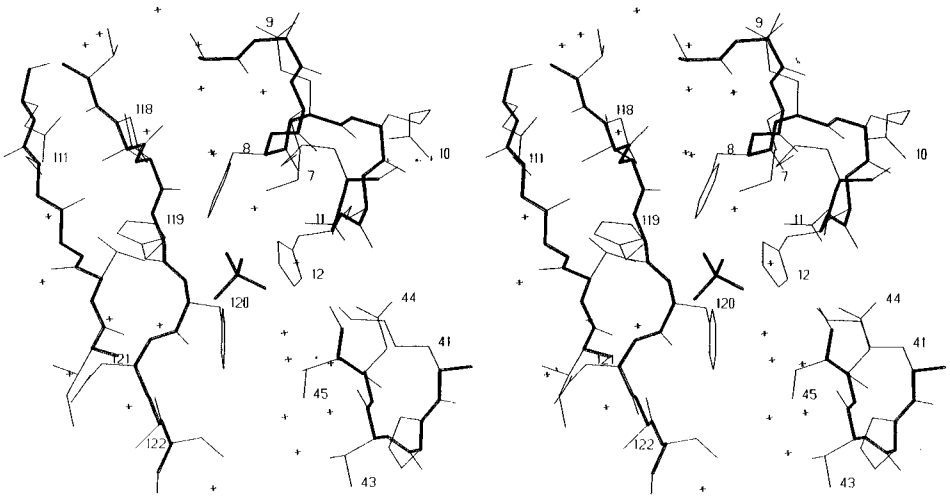

FIGURE 4: Stereoscopic view of the trigonal RNase A (W1) active site with sulfate ion bound.

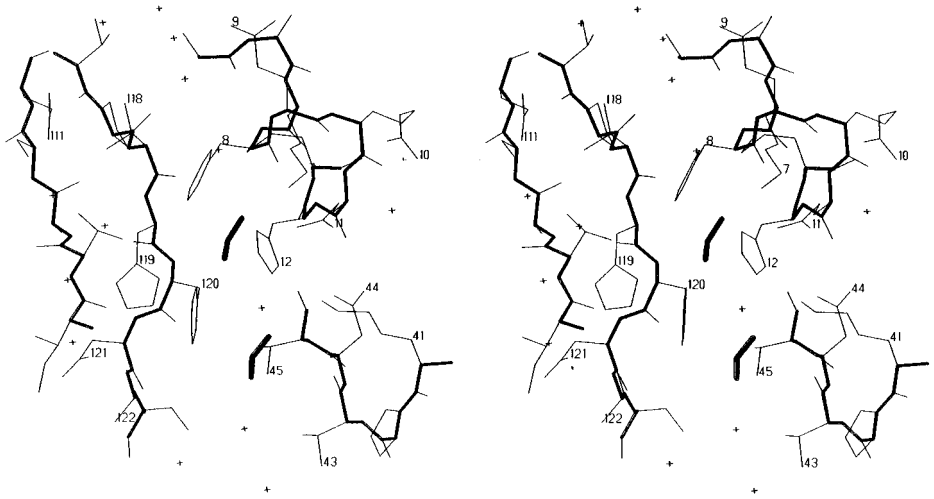

FIGURE 5: Stereoscopic view of the trigonal RNase A (W5) active site with two formate ions bound.

ion (CL-127), bound in the B_1 subsite, forms hydrogen bonds to the backbone amide of Thr 45 and to a water molecule (WAT-279; W4 numbering) (Table 6). CL-127 was found in a similar position in the fluorescent derivative of the trigonal form of RNase, where the crystals were obtained in the presence of 3 M NaCl (Baudet-Nessler et al., 1993). CL-125 is absent in this RNase A derivative due to steric interference of the covalently bound fluorophore.

Crystals prepared from 2.5 M sodium chloride and 3.3 M sodium formate (W6) contain only a single active site chloride ion, CL-127, which is bound in the B_1 site with approximately the same hydrogen-bonding pattern as observed in models W3 and W4 (Table 6). In this structure, CL-125 has been replaced by the water molecule (WAT-201) which refines with full occupancy and a *B*-factor of 15.5 Å^2. WAT-201 in the W6 model has retained the coordination observed for CL-125 in models W3 and W4 with slightly shorter hydrogen bonds (Table 6). The low *B*-factor of WAT-201 suggests that a chloride ion might also be binding at this site with low occupancy, but a water molecule is preferred due to the stable refinement and the lack of residual electron density in difference Fourier syntheses.

Structures obtained from crystals in 80% ammonium sulfate (W1, W2) each have a single sulfate ion (SO4−125) bound in the P_1 position of the active site (Figure 4, Table 6). Oxygen atom O2 of the sulfate ion participates in two hydrogen bonds with NE2 of His-12 and the backbone amide of Phe-120 in both models. Oxygen atom O3 forms a hydrogen bond to ND1 of His-119 in both models W1 and W2. Oxygen atom O4 of the sulfate forms hydrogen bonds to Lys-41 NZ and Gln-11 NE2 in both models. Oxygen atom O1 forms a hydrogen bond to the backbone amide of Phe-120 in the model W2, but due to a slight rotational shift of SO4−125, this interaction is absent in W1. In both structures, SO4−125 also forms three hydrogen bonds to three water molecules in the active site.

The structure obtained in the presence of 8 M sodium formate (W5) contains two formate ions (FMT-131 and FMT-132) bound in the active site (Table 6, Figure 5). FMT-131 is located very close to the substrate phosphate group binding site (P_1), while FMT-132 is bound in the pyrimidine base binding site (B_1). Oxygen atom O1 of FMT-131 forms a single hydrogen bond to NE2 of Gln-11, while O2 forms hydrogen bonds with NE2 of His-12 and the backbone amide of Phe-120. The FMT-131 O2 also participates in a hydrogen bond with WAT-240. Oxygen atom O1 of FMT-132 forms hydrogen bonds with the backbone amide of Thr-45 and WAT-240, while O2 of FMT-132 is hydrogen bonded to Thr-45 OG1. FMT-131 and FMT-132 occupy positions analogous to those of CL-125 and CL-127, respectively, but with different hydrogen-bonding patterns.

The gross features of the active site are preserved in all crystal forms of native trigonal RNase A; however, there

Table 6: Anions Binding in the Active Site of Trigonal RNase A at Different Salt Conditions

	distances (Å)					
hydrogen bond	W1	W2	W3	W4	W5	W6
CL 125···His 12 NE2			3.15	3.14		
CL 125···Phe 120 N			3.31	3.25		
CL 125···WAT 232[a]			3.03	2.86		
CL 125···WAT 279[a]			3.37	3.45		
SO4 125 O1···Phe 120 N		3.34				
SO4 125 O2···His 12 NE2	2.61	2.52				
SO4 125 O2···Phe 120 N	2.91	3.30				
SO4 125 O2···WAT 216[c]	2.71	2.43				
SO4 125 O3···His 119 ND1	2.92	2.87				
SO4 125 O3···WAT 299[b]	2.56					
SO4 125 O4···Lys 41 NZ	3.00	3.53				
SO4 125 O4···WAT 268[c]	2.83	2.68				
SO4 125 O4···WAT 307[c]		3.22				
CL 127···Thr 45 N			3.14	3.35		3.23
CL 127···WAT 279[a]			2.97	3.35		3.07
FMT 131 O1···Gln 11 NE2					2.70	
FMT 131 O2···Phe 120 N					2.91	
FMT 131 O2···His 12 NE2					2.84	
FMT 131 O2···WAT 240[d]					2.96	
FMT 132 O1···Thr 45 N					3.00	
FMT 132 O1···WAT 240[d]					3.03	
FMT 132 O2···Thr 45 OH					2.86	

[a] Waters are numbered as in model W4. [b] Waters are numbered as in model W1. [c] Waters are numbered as in model W2. [d] Waters are numbered as in model W5.

are differences in the detailed conformation, hydrogen-bonding patterns, and ion binding capacity of residues implicated in substrate binding and catalysis.

(A) His-12. His-12 moves very little among the six salt forms studied. His-12 is hydrogen bonded to the carbonyl of Thr-45 through its ND1 in all six trigonal RNase A structures and in the native monoclinic RNase A structure (Wlodawer, 1985).

(B) Gln-11. The side chain of Gln-11, which is involved in substrate and transition state binding, appears to occupy a single rotamer conformation (within approximately 30° on χ_1) in the six trigonal salt forms. Gln-11 NE2 forms a tight hydrogen bond (2.70 Å) to one of the formate ions observed in the trigonal crystals grown in the presence of 8 M sodium formate. The Gln-11 carbonyl oxygen forms a hydrogen bond with Asn-44 ND2 in all six native trigonal RNase A structures and in the native monoclinic RNase A structure (Wlodawer et al., 1988). In native monoclinic RNase A, Gln-11 was the only residue in the region of the P_1 phosphate binding site which was modeled with multiple conformations (Wlodawer et al., 1988).

(C) Lys-7. The side chain of Lys-7, which is thought to constitute part of the P_2 subsite, adopts a similar conformation in all salt forms of trigonal RNase A except for the NZ atom. NZ is directed into the active site cleft in models with highest ionic strength (W1 and W2), while in structures from low ionic strength (W3, W4, W5, and W6), it is directed away from the active site cleft as observed in the native monoclinic RNase A (7RSA). In both conformations, Lys-7 NZ has no interactions with other protein atoms.

(D) Lys-41. The side chain of Lys-41 has well-defined electron density in all six structures of the native trigonal RNase A, and the RMS deviations for the atomic positions of Lys-41 are on average 0.6 Å between native trigonal and monoclinic RNase A (7RSA). Lys-41 NZ forms hydrogen bonds to OD1 of Asn-44 and to a water molecule located in the active site cleft in all salt forms of trigonal RNase A. Lys-41 NZ forms a subsidiary third H-bond with OE1 of Gln-11 in models with the highest ionic strength, which have a sulfate ion bound in the active site (i.e., W1 and W2) . Atomic positions of the Lys-41 side chain have an RMS deviation of 0.6 Å between these two models (W1, W2) and other salt forms. Lys-41 NZ forms an additional H-bond to the Val-43 carbonyl in model W4, which has two chloride ions bound in the active site (Figure 3). The RMS deviations for atomic positions of Lys-41 are on average 0.7 Å between model W4 and other salt models.

(E) Lys-66. Lys-66, a part of the P_0 subsite, forms only a single hydrogen bond between its backbone nitrogen and OD2 of Asp-121 in native trigonal RNase A. The side chain has ill-defined density beyond its CD atom in models W1, W2, W3, and W6 and well-defined density for all its atoms in models W4 and W5. In all models the side chain of Lys-66 is directed away from the active site cleft, and in no case is a hydrogen bond observed between the side chain of Lys-66 and Asp-121. Contrary to these findings, Lys-66 NZ is observed forming hydrogen bonds to the side chain OD1 and main chain oxygen of Asp-121 in the semisynthetic trigonal RNase (Martin et al., 1987). A hydrogen bond between Lys-66 NZ and Asp-121 O was also observed in native monoclinic RNase A (7RSA), where the Lys-66 side chain is directed into the active site cleft.

(F) His-119. As a consequence of direct ligand binding, His-119 adopts different conformations under different ionic conditions (Figure 6, Table 5). Without bound sulfate (W3, W4, W5, and W6), His-119 adopts the A conformation and NE2 of His-119 forms hydrogen bonds with OD1 of Asp-121 and a water molecule, while ND1 of His-119 has no contacts with either protein or solvent. These interactions are similar to those found in native monoclinic RNase A grown from alcohol (7RSA). In the presence of high concentrations of ammonium sulfate (W1, W2), sulfate is discretely bound in the active site and His-119 adopts the B conformation. Under these conditions, ND1 of His-119 forms a hydrogen bond to a sulfate oxygen and NE2 hydrogen bonds to a water molecule (Figures 4 and 6). This hydrogen-bonding arrangement is similar to that observed in semisynthetic RNase A (Martin et al., 1987) and in RNase S (Kim et al., 1992).

Intermolecular Ion Binding Sites. In addition to the principal ion binding sites located at the active site of the native trigonal RNase A (Table 6, Figures 3−5) several other solvent peaks could be interpreted and refined as intermolecular ions. An outstanding peak in the difference $F_o - F_c$ and $2F_o - F_c$ electron density maps of the W1 and W2 structures (80% saturated ammonium sulfate) was modeled as a second sulfate ion. This anion, SO4−126, participates in a total of eight hydrogen bonds (Figure 7). The backbone amides of Ala-4, located at the N-terminus of helix H1, and Ser-23, located at the N-terminus of helix H2 of a molecule related by the screw axis, are the main ligands, each donating a single hydrogen bond to a sulfate oxygen. The third ligand is Ser-23 OG1 from a molecule related by the 2-fold screw axis, which is involved in a bifurcated hydrogen bond to two sulfate oxygens. Three water molecules form four hydrogen bonds to the sulfate oxygens. This pattern of hydrogen bonding is commonly observed for anion-binding sites in proteins (Chakrabarty, 1993).

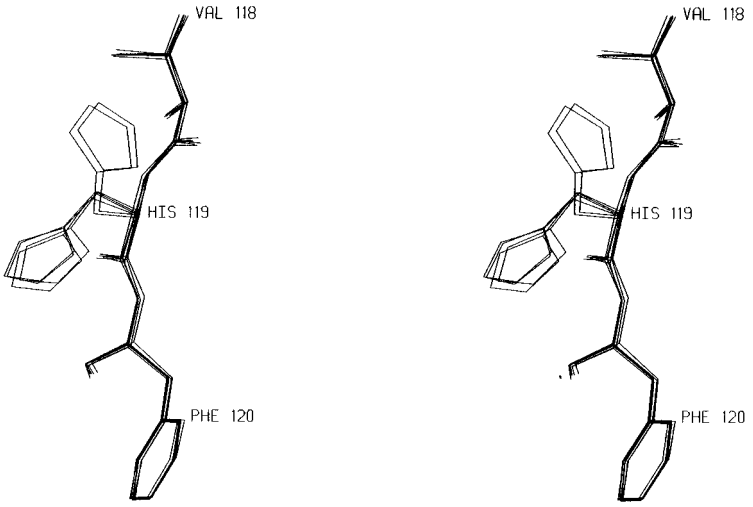

FIGURE 6: Stereoscopic view of the predominant conformation of His-119 in each of the six structures reported here. "Up" conformation was observed in models with highest ionic strength (W1 and W2). "Down" conformation was observed in models with lower ionic strength (W3, W4, W5, and W6).

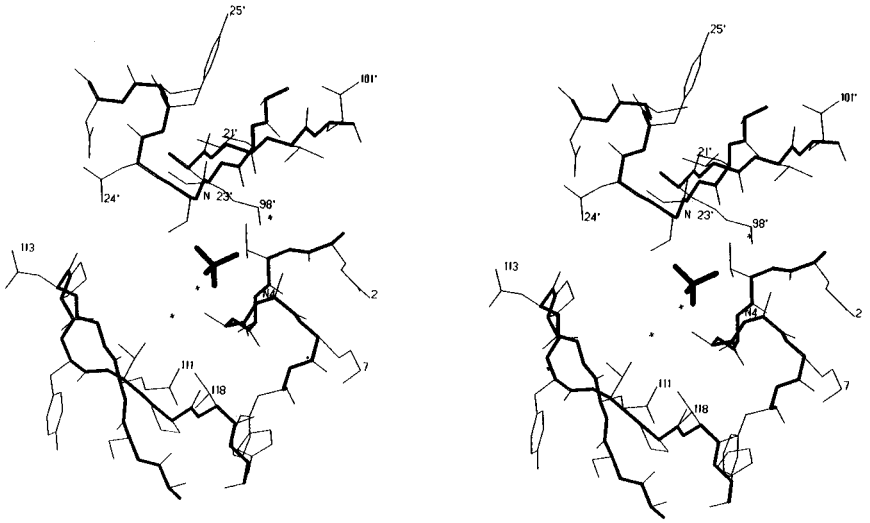

FIGURE 7: Stereoscopic view of the second sulfate ion binding site in trigonal (W1) crystals of RNase A. Only water molecules donating hydrogen bonds to the intermolecular sulfate ion are shown.

In addition to the chloride ions bound in the active site of the structures W3, W4, and W6, two intermolecular chloride ions were identified in each of these structures. The location and coordination of these intermolecular chloride ions are almost identical in these three models and are similar to those found in trigonal crystals of a covalent fluorescent derivative of RNase A (Baudet-Nessler et al., 1993). The first intermolecular chloride ion forms hydrogen bonds to Thr-3 OH and to three water molecules which mediate interactions with Lys-98 NZ and the Thr-99 backbone amide of the molecule related by the 2-fold screw axis. The second intermolecular chloride ion forms hydrogen bonds to Thr-78 OH, Thr-78 O, two water molecules, and Asn-34 ND2 of the molecule related by the 3-fold screw axis (Figure 8).

Crystals grown from cesium-containing solutions are normally transferred to concentrated ammonium sulfate prior to mounting in order to reduce X-ray absorption caused by cesium. This procedure was used in this study for forms W1 and W2 of native trigonal RNase A (Table 1). However, crystals of form W3, containing 3 M CsCl, were mounted directly without removal of cesium. Refinement of W3 starting from the W1 model resulted in an *R*-factor of 17.5% for data in the range 8.0−2.0 Å. This *R*-factor is the poorest among the structures reported, possibly due to absorption effects (Table 2). All outstanding peaks in difference Fourier syntheses were examined for density attributable to bound Cs^+. The cation has 55 electrons and at full occupancy should be easily distinguished from chloride anions that have 18 electrons. Only a single peak over 6σ was found. In model W4, obtained in the presence of 3 M NaCl (all other conditions were identical to W3), a water molecule is located in this position. Modeling the peak in the difference maps for W3 as a water molecule resulted in an unrealistically low *B*-factor and residual electron density. This peak could be satisfactorily modeled as a Cs^+ ion, which refined to an occupancy of 0.32 and a *B*-factor of 21.5 Å^2. Subsequent difference Fourier syntheses showed no residual features in this region. We favor assignment as a cesium cation because the spherical nature of the electron density is not consistent with a sulfate ion and the coordinating ligands are incompatible with a chloride anion.

The cesium ion interacts with two main chain carbonyl groups: Thr-78 O and Ser-32 O from a symmetry-related molecule at distances of 3.01 and 3.08 Å, respectively. Cs^+ is located approximately in the plane of the two peptide bonds. The cesium cation is within 4 Å of both Asp-49 OE2

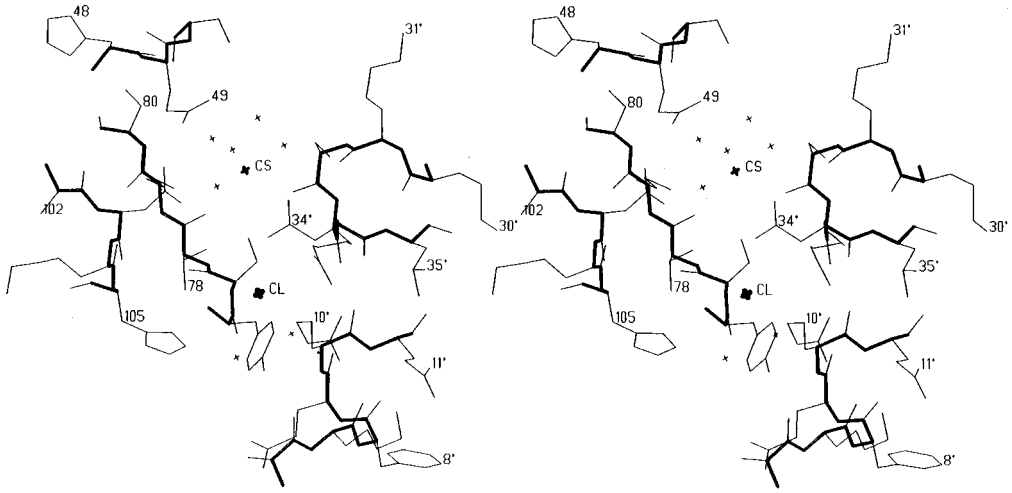

FIGURE 8: Stereoscopic view of the Cs^+ and Cl^- intermolecular binding site in W3 crystals of RNase A.

FIGURE 9: Cross-linking of symmetry-related molecules by ions in the trigonal RNase A crystal structure, space group $P3_221$. (A, top) Sulfate ions mediating interaction between molecules, related by a 2_1 screw axis parallel to the *b*-axis of the unit cell. (B, bottom) Chloride anion and cesium cation mediating interactions between molecules related by the 3_2 screw axis parallel to the c-axis of the unit cell. Small filled circles are Cs^+ ions, and larger filled circles are Cl^- ions.

of one molecule and Asn-34 OE1 of the symmetry (3_2) related molecule (Figures 8 and 9). Five water molecules form hydrogen bonds to the Cs^+ cation, which mediate interactions with Asp-49 OE1, Asp-49 OE2, Asp-53 OD2, the carboxamide group of Gln-103, and the carbonyl of Ser-32 from a symmetry-related molecule. The geometry and the coordinating ligands around the cesium cation are typical for metal ions binding in proteins (Chakrabarty, 1990a,b).

Crystal Packing. Figure 10 shows the packing of the RNase A molecules in the trigonal crystal lattice. This crystal form has a solvent content of 59%, the highest among all known RNase crystal forms (Crosio et al., 1992). Large solvent channels, with 3-fold symmetry and a diameter of 40 Å, are centered at each corner of the unit cell running parallel to the crystallographic *c*-axis. The active site faces this channel and is thus highly solvent accessible. Each RNase A molecule makes intimate contacts with five symmetry-related neighbors (see Table 7 for hydrogen-bonding and salt bridge contacts between symmetry-related molecules in crystals of trigonal RNase A).

The largest interface is formed between one molecule and the 2-fold related symmetry mate. The 2-fold axis of

Table 7: Intermolecular Hydrogen Bonds and Salt Bridges in the Trigonal RNase A Crystals[a]

	residue in		distance (Å)					
symmetry transformation	molecule 1	molecule 2	W1	W2	W3	W4	W5	W6
$1-Y, X-Y, Z-{}^1/_3$	Glu-9 OE2	Lys-61 NZ	3.04	2.82	2.84	2.77		2.82
	Ser 32 O	Ser-77 OG	2.89	2.95	3.25	3.10	3.27	3.13
	Asn-34 ND2	Ser-77 OG	3.30	3.36				
	Asn-34 ND2	Thr-78 OG1	3.23	3.29	3.26	3.14	3.36	3.20
	Cl-126	Thr-78 N			3.35	3.35		3.52
$Y, X, 1-Z$	Asn-62 O	Gly-88 N	3.35	3.44	3.32	3.34	3.20	3.36
	Ala-64 N	Glu-86 O	2.99	3.00	2.84	2.92	2.88	2.85
	Ala 64 O	Arg-85 NH1	2.84	2.75	2.85	2.80	2.84	2.85
	Gln 74 OE1	Thr-100 OG1				3.43		3.45
	Arg-85 NH1	Asp-121 OD2	2.81	3.00	3.22	2.94	2.94	3.06
	Lys-104 NZ	Lys-104 NZ	2.72	2.68	2.34	2.31	2.60	2.36
	Lys-104 NZ	Val-124 OT1	2.88	3.54	3.44	3.13	2.96	3.21
$1-X, 1-X+Y, {}^2/_3-Z$	Ser-23 N	SO4 126 O3	2.95	3.32				
	Ser-23 OG	SO4 126 O3	3.11	3.49				

[a] Water-mediated hydrogen bonding interactions are not included.

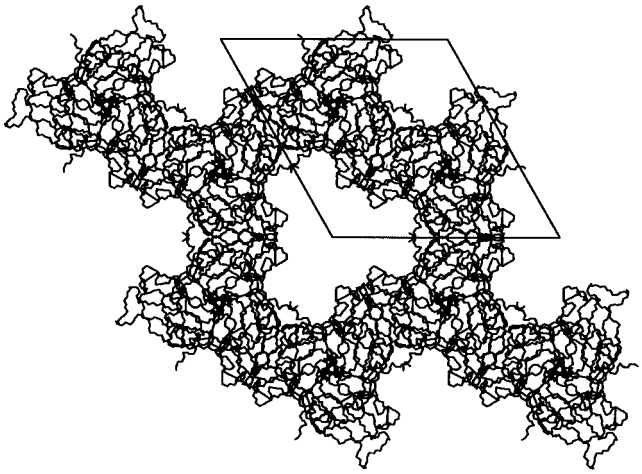

FIGURE 10: Packing of RNase A molecules in trigonal crystals of the W form. The diagram is viewed along the crystallographic *c*-axis.

symmetry runs along the diagonal of the *XY* plane of the unit cell. Figure 11 shows the details of the intermolecular contacts looking down the 2-fold axis. Two main chain to main chain hydrogen bonds between β-strand 62−64 of one molecule and the antiparallel β-strand 88−86 of the neighboring molecule provide a major contribution to the stabilization of the dimer (Table 7, Figure 11). An almost identical dimer is observed in all crystal forms of RNase obtained in high salt (Crosio et al., 1992), and a similar dimer is seen in monoclinic RNase B crystals grown from poly(ethylene glycol) at low ionic strength (Williams et al., 1987). As seen in Figure 11, the active site clefts of two dyad-related molecules are closely coupled about this axis. The side chain of Arg-85 protrudes into the active site of the dyad-related molecule, forming a salt bridge to Asp-121 and a hydrogen bond to the Ala-64 carbonyl group.

A seemingly unfavorable ionic interaction occurs between Lys-104 NZ atoms of the two dyad-related molecules (2.3−2.7 Å; Table 7). The Ser-123 carbonyl group of one molecule and Val-124 carboxyl groups of both molecules are located in close vicinity of each Lys-104 NZ and may stabilize this arrangement. A similar close interaction between symmetry-related Lys-104 side chains is observed in dimers of RNase S (files 1RNV and 1RNU from PDB), semisynthetic RNase A and its derivatives (1SRN, 3SRN, 4SRN), RNase B (1RBB), and fluorescent derivatives of RNase A (1RAS, 1RAR). A larger distance (3.8 Å) between Lys-104 side chain NZ atoms is found in crystals of covalent nucleoside derivatives of RNase A, where the crystallographic 2-fold axis is replaced by a local dyad (Nachman et al., 1990). The close (2.3−2.7 Å) approach of NZ atoms of the two lysines makes it unlikely that both side chains are positively charged. One of the lysines may have an aberrant pK_a value near 5.5, the pH of the current structure determinations. There is precedence for such dramatically perturbed pK_a values, as one of the active site lysines in acetoacetate decarboxylase has a pK_a of 6.0 (Kokesh et al., 1971). There is also precedence for the close (2.3−2.7 Å) approach of lysine side chains in protein crystals. A distance of 2.7 Å between symmetry-related Lys NZ atoms was observed in crystals of BPTI (Gallagher & Croker, 1994), and a distance of 2.3 Å was reported in the active site of transferrin (Dewan et al., 1993). It has been suggested that these close contacts represent low-barrier hydrogen bonds, and the lysine pair in RNase A may provide another example.

The packing of molecules related by the 3-fold screw axis is mediated by chloride ions in crystal forms W4 and W6 and chloride and cesium ions in crystal W3. These ions are bound between symmetry-related molecules within the lattice and probably contribute to the formation and maintenance of the crystal. A salt bridge is formed between Glu-9 OE2 and Lys-61 NZ from a molecule related by the 3_2 screw axis in all crystal forms except form W5 (8 M sodium formate), where the side chain of Lys-61 adopts a different orientation. An additional intermolecular hydrogen bond between Asn-34 ND2 and Ser-77 OG1 across the 3_2 screw axis is present only in the W1 and W2 forms (highest ionic strength) due to the different conformation of the Ser-77 side chain in these crystals (Table 4).

Water Molecules. The solvent structure was refined independently for each of the six models of native trigonal RNase A. Table 8 shows the number of waters that occupy similar positions in the six trigonal and the monoclinic forms (file 7RSA) of the native RNase A. After least squares superposition of the backbone atoms, solvent molecules were considered to be equivalent if the oxygen atoms were within 1 Å of each other and made similar interactions with their neighbors. Comparison of the water molecules in the six trigonal crystal forms of RNase A shows that 48 are found

FIGURE 11: Interface between two RNase A molecules at the 2-fold axis in trigonal crystals of native RNase A W1 form crystals. Only carbonyl groups and side chains (thin lines) at the intermolecular interface are shown.

Table 8: Water Molecules Closer than 1 Å Apart in Six Trigonal and One Monoclinic Form (7RSA) of Native RNase A[a]

RNase A structure	W1	W2	W3	W4	W5	W6	7RSA
W1	112	72	64	66	64	62	60
W2		110	66	77	60	71	63
W3			99	71	52	68	60
W4				103	66	78	64
W5					89	60	56
W6						95	63
7RSA							188

[a] The numbers on the diagonal correspond to the total number of water molecules in the structure. The numbers in the upper triangular part of the matrix indicate the number of waters considered structurally equivalent in the two structures. The table does not include positions occupied by ions in trigonal RNase A.

in similar positions in all six models while 62 are found in five models and 78 in four models. Seven of the fully conserved waters are involved in intermolecular contacts. Comparison of solvent positions in the six trigonal forms and the monoclinic form (7RSA) shows that 41 solvent sites are conserved in all seven models, 58 solvent sites are conserved in six out of seven structures, and 71 are conserved in five out of seven structures. Figure 12 shows the 48 conserved solvent sites in the six native trigonal RNase A structures.

All ions replace previously identified water molecules, thereby conserving the occupancy of these sites. WAT-201 in model W6, CL-125 in models W3 and W4, oxygen atom O2 of the sulfate 125 in models W1 and W2, and the oxygen atom O2 of the FMT-131 in model W5 all occupy a similar location in the active site (P_1 subsite). The second conserved position in the active site (B_1 subsite) is occupied by CL-127 (W3, W4, W6), oxygen atom O1 of the FMT-132 (W5), WAT-204 (W1), and WAT-215 (W2). A conserved intermolecular position is occupied by CL-126 (W3, W4, W6), WAT-259 (W1), WAT-258 (W2), and WAT-210 (W5). The second intermolecular chloride ion, CL-128, bound near the N-terminal part of helix H1 in models W3, W4, and W6, displaces water observed in all other models [WAT-218 (W1), WAT-216 (W2), and WAT-225 (W5)].

The oxygen atom O1 of FMT-131 occupies the approximate position of waters in all other models. It is interesting to note that oxygen atom O2 of FMT-132 (W5) is substituted by waters in the models with highest ionic strength, WAT-227 (W1) and WAT-282 (W2), while no water molecules were present at this position in models with low ionic strength (W3, W4, and W6). The cesium cation bound in model W3 displaces water molecules found in all other models. Water molecules in models W3, W4, and W6 occupy similar positions as the sulfur atom of the intermolecular SO4-126 in models W1 and W2, although with longer hydrogen bonds to the backbone nitrogen atom of Ala-4 than those formed by sulfate oxygens.

Electrostatic and Ionic Interactions. Electrostatic surface potential calculations reveal an almost continuous band of positive potential running around the RNase A molecule (Figure 13). The positive potential runs up through the active site (including residues Lys-1, Lys-7, Arg-10, His-12, His-119, Lys-41, Lys-66, and Lys-104) and winds around the molecule (including Lys-31, Arg-33, Lys-37, Lys-91, Arg-85, and Lys-98). The only intramolecular salt bridge conserved in all the structures is the interaction between Glu-2 and Arg-10 on the amino-terminal α-helix. The majority of the ionizable groups do not participate in ionic interactions.

Functional Group Maps. The presence of two bound formates (i.e., carboxylate functionalities) in the W5 structure allowed for a direct experimental test of the MCSS method. An MCSS search, carried out with a formate probe, found one of these sites (site 1, the equivalent of FMT-131) as a very low energy minimum but did not locate the other (site 2, the equivalent of FMT-132). While many formate minima (33) were located on the W5 structure, the lowest energy ones were in the active site. The minimum corresponding to site 1 was "essentially" the lowest energy minima found; there was one lower energy minimum, but it is an artifact of the poorly defined side chain position of Lys-1. The calculated interaction energies of FMT-131 and FMT-132 with the protein are −117.4 kcal/mol and −67 kcal/mol, respectively. Although the interaction energy of site 2 is only about half that of site 1, site 2 still has a substantial negative interaction energy and was expected to be identified by the MCSS search. This discrepancy was resolved by explicitly placing a formate at site 2 in the protein and energy minimizing, holding the protein fixed. The energy dropped to −155.3 kcal/mol, but surprisingly this formate moved >5 Å to occupy almost the same position as site 1 (difference in OD2 atoms is only 0.44 Å). Thus, in an unbiased search, site 2 is never found because both sites reside in roughly

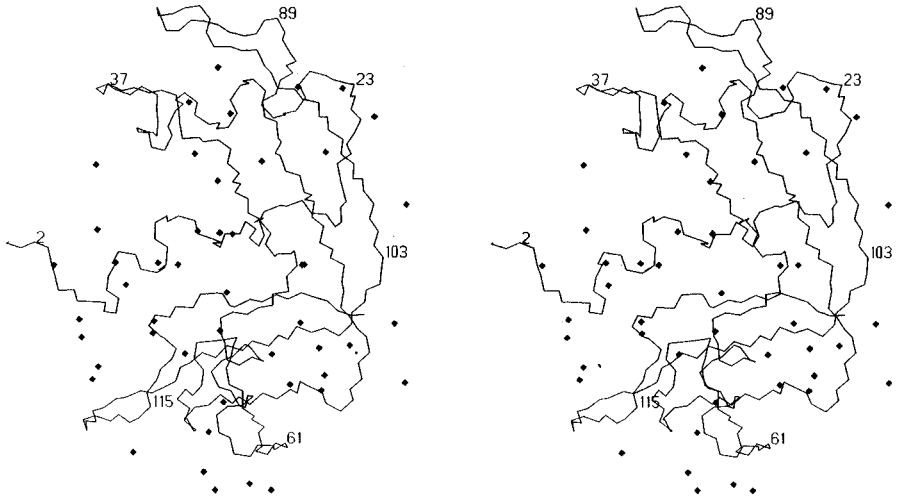

FIGURE 12: Conserved solvent sites in six native trigonal RNase A structures.

the same potential energy well and a formate anion initially placed at site 2 minimizes to the position of site 1. As confirmation of this, an MCSS calculation was performed with site 1 explicitly occupied, and a minimum corresponding to site 2 was indeed found.

DISCUSSION

Effect of Ionic Strength on Overall Structural Features. The refined structures of native RNase A in the trigonal form W all show a very similar backbone structure regardless of ionic conditions. In particular, the structure of the recombinant protein (W2) is essentially the same as the bona fide protein from bovine pancreas (W1) (RMS = 0.18 Å). This is the first report of the structure of a recombinant RNase A and shows that structure−function studies on RNase A are indeed feasible. These native structures also show little difference from the semisynthetic RNase W (1−118, 111−124), confirming that the introduction of the covalent break has little effect on the overall structure.

A comparsion of these high salt crystal structures with the 1.26 Å monoclinic structure from alcoholic solution shows that the detailed tertiary structure is conserved as are all elements of secondary structure. Crystallographic studies on other single domain proteins including T4 lysozyme (Bell et al., 1991), cytochrome *c* (Sanishvilli et al., 1995), BPTI (Wlodawer et al., 1987a,b), trypsin/trypsinogen (Bode & Huber, 1978), hen egg white lysozyme (Moult et al., 1976), and human profilin (A. A. Fedorov and S. C. Almo, unpublished results) under different ionic conditions have produced similar results. These findings reinforce the belief that protein structure is generally uneffected by the composition of the mother liquor and that structures determined from crystals grown in high salt exhibit the overall features present under physiological conditions.

Effect of Ionic Strength on Electrostatic and Polar Interactions. While the main chain conformation of RNase A appears insensitive to solvent conditions, there is some variability in polar and side chain interactions. The only intramolecular salt bridge present in all seven RNase A structures is the interaction between Glu-2 and Arg-10 located on the amino-terminal α-helix. This interaction is favored due to the *i*,*i*+8 positioning of these residues, which places the complementary charges of the side chains on the same face of the helix. Trigonal forms W3, W4, W5, and W6 and the monoclinic form have an electrostatic interaction between His-119 and Asp-121. In these crystal forms the active sites are occupied by either water, formate, or chloride. In the W1 and W2 structures, His-119 forms a tight ionic interaction with a sulfate anion bound in the active site which prevents an interaction with Asp-121. The majority of the differences in salt bridges involve crystal contacts, direct binding of ions, or the presence of long (and therefore weak) interactions. Though one might predict a decrease in ionic strength to lead to the formation of additional, or stronger, salt bridges, the RNase A structures do not provide any evidence of this. Consistent with this are the high-resolution studies of three isomorphous salt forms of T4 lysozyme which also did not identify any change in ionic interactions (Bell et al., 1991). These findings suggest that ionic strength is not a major determinant of ion pair formation on a protein surface and indicate that protein structures derived from high salt crystals provide suitable models for electrostatic calculations.

The side chain conformation of some residues in RNase A is responsive to the ionic composition of the mother liquor. In the active site, Lys-7, Lys-41, and Lys-66 show some differences in side chain conformation and/or hydrogen-bonding patterns. Of particular importance is His-119 for which two distinct conformations have been described in certain RNase A crystal structures. Borkakoti et al. (1982) observed two discrete conformations for His-119, denoted A and B, in crystals grown from alcohol solutions (see Table 4). Conformation A, the so-called down position, has torsion angles $\chi_1 = 149°$ and $\chi_2 = 106°$ and an occupancy of 0.8. Conformation B, the up position, has torsion angles $\chi_1 = -76°$ and $\chi_2 = -55°$ and an occupancy of 0.2. Other reports support the existence of only the A conformation in native monoclinic RNase A in either the absence of sulfate or presence of sulfate at low ionic strength (Wlodawer et al., 1983, 1988; Campbell & Petsko, 1987). Only the B conformation was observed in crystals of RNase S (Kim et al., 1992) and semisynthetic RNase W (Martin et al., 1987), both of which were prepared from 80% ammonium sulfate. Clear evidence of the simultaneous presence of the A and B conformations of His-119 was found in one subunit of bovine seminal ribonuclease dimer (80% identity with RNase A), while only the B conformation was observed in the second

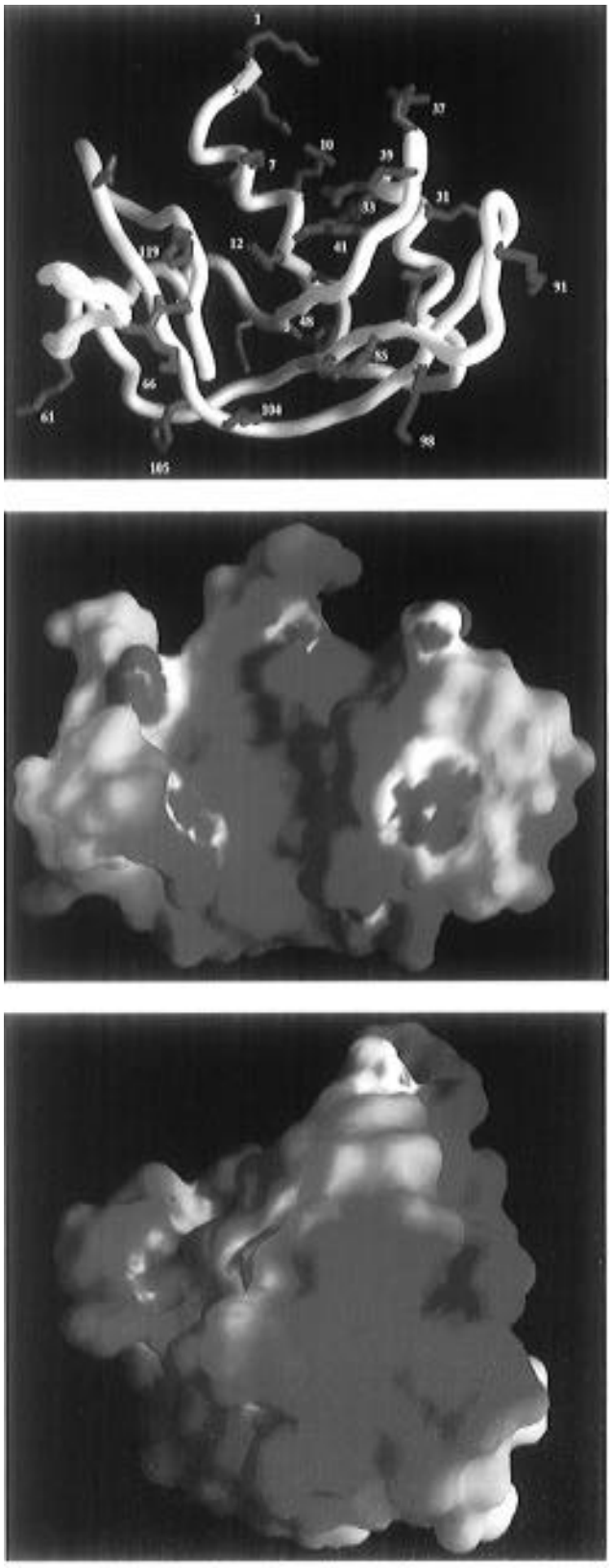

FIGURE 13: (A, top) Backbone model of RNase A showing the basic (blue) and acidic (red) side chains. (B, middle) Electrostatic potential surface of RNase A in the same orientation as panel A, displayed with GRASP at $\pm 4kT$. Blue and red represent regions of positive and negative potential, respectively. (C, bottom) Electrostatic potential surface of RNase A oriented approximately 90° about the vertical axis relative to panel A.

subunit of the dimer (Mazzarella et al., 1993). Crystals of bovine seminal ribonuclease were also prepared in 80% ammonium sulfate (Mazzarella et al., 1993).

Mobility and Catalysis. The predominant conformations of His-119 found in trigonal native RNase A structures at pH 5.5 under different ionic conditions are shown in Figure 6. His-119 uniquely adopts the B conformation when sulfate is bound at the active site. All other structures show only the A conformation. Based on model building, it has been previously suggested that His-119 in either the A or B conformation could effectively catalyze transphosphorylation (deMel et al., 1991). Direct examination of the productive binding mode the dinucleotide d(CpA) (A. A. Fedorov and S. C. Almo, unpublished results) suggests this is not the case. If His-119 occupied the B conformation, there would be extensive steric conflict with the purine base forcing the dinucleotide to adopt a noncanonical conformation. Despite this, the extensive mobility of His-119, as well as the small scale motions of other active site residues, may be required for efficient catalysis.

The importance of conformational flexibility has been previously considered with specific regard to RNase A (Alber et al., 1973) and is likely to be a common feature of enzymes. As the reaction coordinate is traversed, the steric and electronic properties of bound substrate are modified, and the active site conformation must respond to allow for stabilization of the transition state. Conformational flexibility is also required for enzymes which recognize different substrates. More extensive active site plasticity is likely to be required for enzymes involved in the catalysis of multiple reactions and multistep reactions. RNase A catalyzes both transphosphorylation and cyclic nucleotide hydrolysis, and the transition states for these two reactions differ, requiring alterations in the active site geometry for optimal stabilization of each. An analogous situation is found with the serine proteases, where the same active site must adapt to allow transition state stabilization for both acyl-enzyme formation and acyl-enzyme hydrolysis.

Mode of Anion Inhibition. Early work showed that the inhibitory behavior of monovalent anions such as chloride and nitrate was consistent with competitive inhibition (i.e., $K_I = 1.4$ and 0.51 M, respectively) (Irie, 1965). However, thermodynamic arguments have been presented which are inconsistent with competitive inhibition and instead point to a more general electrostatic screening mechanism to account for the observed pattern of inhibition (Bolen et al., 1971). The current results bear on these issues, as high occupancy binding of both chloride and formate anions is observed in the active site. Both of these anions are observed to bind in two distinct, nonoverlapping active site locations. CL-125 interacts with His-12 and the backbone amide nitrogen of Phe-120 in the P_1 site, while CL-127 interacts with the backbone of Thr-45 in the B_1 specificity pocket. Likewise, FMT-131 and FMT-132 bind in the P_1 and B_1 sites, respectively. Interestingly, CL-125 and FMT-131 O2 occupy a position almost identical to that of the equatorial oxygen (O8) in the uridine vanadate transition state analog structure (Borah et al., 1985). While electrostatic screening might play a role in the mechanism of inhibition, the observation of high occupancy binding in the major ligand subsites argues that direct competition for substrate binding contributes to the inhibitory behavior of monovalent anions.

Extended Binding Sites. Of particular importance is the identification of the subsites occupied by extended oligonucleotide ligands. As sulfate mimics the properties of phosphate, it may be used to map the surface of the RNase

A molecule for potential phosphate binding sites. In addition to SO4−125 bound at the P_1 site, only one additional sulfate, SO4−126, is observed at an intermolecular site. SO4−126 receives hydrogen bonds from the backbone amide nitrogen of Ala-4 and further interacts with the dipole moments associated with helices of symmetry-related molecules in the crystal. Interestingly, a sulfate is found in a similar intermolecular position, with similar ligands in the bovine seminal ribonuclease crystal structure (Mazzarella et al., 1993); however, SO4−126 is distant from the predicted positions of the P_0, P_2, P_3, and P_1' subsites (Figure 1) (de Llorens et al., 1989), and the relevance of this site is unclear. The finding of only a single additional sulfate site suggests that, with the exception of the P_1 subsite, individual RNase A−phosphate interactions are weak. Occupancy of additional subsites likely requires the cooperative interactions available from polynucleotide ligands. The additional phosphate subsites are likely to be formed, at least in part, by solvent-accessible basic residues.

There is a systematic distribution of amino acids, with nearly all of the basic residues located in an almost continuous band of positive electrostatic potential (see Figure 13). The band of positive potential runs through the active site cleft and spans the circumference of the molecule, suggesting an extended binding site for polyanions. Preliminary modeling studies indicate that, in a fully extended conformation, a polynucleotide ligand of eight nucleotides could be accommodated. The existence of extended binding sites on the enzyme for base, ribose, and phosphate groups (i.e., the B_n, R_n, and P_n subsites) is supported by kinetic studies showing enhanced cleavage of extended substrates (Sawada & Irie, 1969; Li & Walz, 1974; Irie et al., 1984a; Irie, 1984b; Katoh et al., 1986) and by direct binding studies (Record et al., 1976; Guasch et al., 1984) and modeling studies (de Llorens et al., 1989). The existence of an extended polynucleotide binding site is also consistent with the observed salt dependence of poly(uridylic acid) cleavage, which points to a number of ionic interactions between RNase A and large nucleic acids (Irie, 1984b). The clustering of basic residues around the active site provides a possible mechanism for directing small and large polyanionic ligands into the active site. A large number of these basic residues are not involved in salt bridges, and the absence of these ionic interactions may facilitate the interaction of these functionalities with extended polynucleotide ligands. This large binding surface may also allow substrates and/or enzyme to adopt a conformation which optimizes catalytic efficiency. Importantly, the catalytic efficiency of RNase A is known to be sensitive to the occupancy of the P_0, B_2, and B_3 sites, all of which are distant from the site of chemistry (Irie et al., 1984a,b). It is well documented that enzymatic activity is dramatically affected by subsite occupancy in diverse families of enzymes, including restriction endoncleases, lysozymes, and the serine and aspartyl proteases. It may be that many enzymes which act on polymeric substrates have evolved a common strategy to utilize the binding energy of these distant subsites to facilitate chemical bond cleavage.

The region of positive electrostatic potential on the surface of RNase A may also provide a mechanism for the limited unfolding of large RNA substrates with weak secondary and tertiary structure and thereby enhance the accessibility of specific cleavage sites on the RNA. This suggestion may be relevant to angiogenin, a member of the ribonuclease superfamily with ∼30% sequence identity to RNase A, which has been implicated as a growth factor involved in blood vessel formation (Kurachi et al., 1985; Strydom et al., 1985). Evidence has accrued which suggests that angiogenin is internalized at the cell surface and transported to the nucleolus where it may catalyze site-specific cleavage of large RNA molecules leading to a developmental program for blood vessel formation (Moroianu & Riordan, 1994). In angiogenin, basic residues are conserved at many of the corresponding positions of RNase A, suggesting that extended binding may be important for angiogenin function.

Solvent Structure. All six trigonal forms contain ∼100 discrete water molecules and the monoclinic form almost twice this number (Table 8). The larger number of ordered watered molecules in the monoclinic form is a consequence of the higher resolution of that structure. Forty-one of the water molecules are observed in all seven RNase structures (Figure 12). The displacement of individual water molecules is not generally correlated with any significant structural change, with the exception of those waters that are directly displaced by ions. The conserved waters tend to be those with the lowest *B*-factors, indicating they are the most tightly bound. A cluster of four water molecules mediates interactions between the amino-terminal α-helix and C-terminal segment 110−121, which contain the catalytic general acids/bases, His-12 and His-119. Another cluster of seven waters stabilizes interactions between helix H3 and the chain segment 73−79. Regions 19−22, 63−69, and 88−95 have only a few conserved solvent sites, consistent with the high temperature factors of these segments. The conserved solvent sites in native trigonal RNase A are also quite similar to those observed for several monoclinic structures of RNase A (Lisgarten et al., 1993), suggesting a structural or functional role.

The three structures of T4 lysozyme determined from crystals prepared in low, medium, and high ionic strength had 96, 113, and 141 waters, respectively (Bell et al., 1991), with 73 common to all three structures. The triclinic (Moult et al., 1975) and tetragonal (Phillips, 1968) crystal forms of hen egg white lysozyme grown under different ionic conditions have appoximately 110 and 140 water molecules, respectively, of which approximately 60 are in common. The three crystal forms of BPTI have between 60 and 70 waters, of which only 16 are common to all (Wlodawer et al., 1987a,b). While lattice contacts may account for the differences observed between different crystal forms of hen egg white lysozyme and BPTI, respectively, this cannot explain the findings with T4 lysozyme and the trigonal forms of RNase A, which involve the comparison of isomorphous crystal forms. At least some of the discrepancy is attributable to interpretation and noise in Fourier syntheses, but there do seem to be differences related to the ionic composition of the mother liquor. It is likely that the most highly conserved crystallographic waters represent bound waters in solution. In light of the above observations, however, care is required in accessing the contribution of "crystallographically bound" waters to catalysis, ligand binding, and protein stability. Recent advances in two-dimensional NMR techniques allow for the identification of bound water, though this normally amounts to a small fraction of those observed crystallographically. These waters are typically internal and

thus the most tightly bound. NMR requires that the water in question have a long residence time (>0.2 ns; Clore et al., 1990) for observation, while crystallography is independent of residence time and requires a high time-averaged occupancy of water to provide detectable electron density. As such these two techniques are complementary and together are likely to provide a more meaningful description of protein hydration.

Functional Group Maps. Extensive effort has been expended in computational methods to aid in the drug discovery process. One approach has centered around the mapping of different functional groups to energetically favorable positions on the surface of a protein. Once identified computationally, these functional groups can be synthetically coupled to provide a novel therapeutic. Fitzpatrick et al. (1993, 1994) have suggested an experimental analog to this computational approach. By placing cross-linked crystals of subtilisin Carlsberg in neat solutions of the water-miscible solvent acetonitrile, they identified a number of acetonitrile molecules, including four bound in the active site at the P_1, P_2, and P_3 subsites. It was further proposed that the use of other water-miscible solvents would identify binding sites for additional functionalities. This approach is limited to the study of functional groups present in liquid solvents (Allen et al., 1996).

The present work identified two formate anions (W5), a carboxylic functionality, bound in the P_1 and B_1 subsites, in aqueous solution. This demonstrates that the experimental functional mapping approach can be extended to include the binding of solutes in aqueous solution when a sufficiently high solute concentration can be achieved. The finding that two different probes (i.e., functional groups) show preference for binding the active sites in two unrelated enzymes is intriguing. These observations may be indicative of the general ease with which active site solvent structure can be displaced in favor of ligands. Such ready desolvation of an enzyme active site must be an important consideration for efficient catalysis.

The identification of bound formate ions in RNase A grown from 8 M formate has allowed for a direct experimental challenge of computational functional mapping techniques. The MCSS algorithm was partially successful in predicting the formate binding sites. FMT-131, the tight binder (interaction energy of −117 kcal/mol), was correctly identified; however, FMT-132 (interaction energy of −67 kcal/mol) was only located after the explicit inclusion of FMT-131 in the starting model. This behavior is understood by realizing that the two formate positions actually reside in the same shallow potential well associated with a local minimum at the position of FMT-131. Only by explicitly including FMT-131 in the calculation, and thereby changing the effective shape of the potential, can the correct location of FMT-132 be identified. These calculations point to an ordered binding mechanism, where FMT-131 must bind first in order to promote the subsequent binding of FMT-132. This observation suggests that similar computational approaches hold promise for the analysis of enzymatic reactions which follow ordered binding mechanisms.

These findings, which are described in detail elsewhere (Joseph-McCarthy et al., 1996), have important implications for the application of computational methods, as drug discovery by functional mapping is intended to identify a number of potentially useful sites, not only the best single site. When a calculation is performed on the protein alone, the best minimum energy positions (or preferred binding sites) will be found; however, to find secondary allowed sites, the calculation must be carried out iteratively with the best sites explicitly occupied. This is equivalent to performing the calculation with part of an inhibitor bound, in order to identify additional functional groups which may yield a tighter binding species.

Crystal Contacts. The form W crystals offer many desirable features for the study of enzyme−ligand complexes. The active site of RNase A is highly accessible in this trigonal crystal form, as it resides on a 40 Å wide solvent channel which runs the entire length of the crystal. The high symmetry of this crystal form ($P3_221$) allows for very efficient data collection strategies. A major consideration for crystallographic studies of RNase A is the removal of the inhibitory sulfate/phosphate from the P_1 subsite (Campbell & Petsko, 1987; Wlodawer et al., 1988). Not only can high concentrations of sulfate compete with ligand binding but the occupancy of the P_1 subsite by sulfate is associated with the formation of nonproductive binding modes for mononucleotide and dinucleotide ligands (Aguilar et al., 1991, 1992; A. A. Fedorov and S. C. Almo, unpublished results). This is of particular concern for the W form crystals described here, as they were initially reported from 80% saturated ammonium sulfate ($\mu = 12.5$) (i.e., W1, W2). Using only 30% saturated ammonium sulfate supplemented with either 3 M CsCl (W3) or 3 M NaCl (W4) ($\mu = 7.0$), we have replaced the sulfate at the P_1 site with a chloride anion. The production of these crystals in 8 M formate ($\mu = 8.0$) with no sulfate present was expected to result in an empty active site. Surprisingly, under these conditions two formates were found in the active at the P_1 and B_1 sites. Like sulfate, the presence of formate in the P_1 site leads to the formation of a nonproductive binding mode for dinucleotide ligands (A. A. Fedorov and S. C. Almo, unpublished results). We have also produced this crystal form at 2.5 M NaCl and 3.3 M sodium formate ($\mu = 5.8$), which provides an active site with only a water molecule bound at the P_1 site. The ability to control anion binding in the active site, combined with the accessibility of the active site and the high symmetry of this crystal form, has allowed for the structural study of a number of RNase A-ligand complexes prepared by either diffusion or cocrystallization (A. A. Fedorov and S. C. Almo, unpublished results). These features will allow this system to be exploited for future structural work, including the possibility of time-resolved crystallographic studies of productive enzyme−substrate complexes.

Conclusions. The structural consequences of mother liquor ionic composition have been examined in crystalline RNase A. No large-scale alterations are observed, consistent with the notion that structures determined under high salt conditions are relevant to the structural and electrostatic properties present under physiological conditions. The ionic composition of the media, however, does lead to a number of subtle changes involving altered patterns of hydrogen bonding and water structure. In the case of RNase A several of these differences are apparent at or near the active site. This suggests that care must be taken when evaluating the detailed active site structure of an enzyme from a single crystal form. These studies provide direct evidence that monovalent anions behave, at least in part, as true competitive inhibitors and have allowed for the experimental

validation of computational methods aimed at identifying ligand binding sites.

REFERENCES

Aguilar, C. F., Thomas, P. J., Moss, D. S., Mills, A., & Palmer, R. A. (1991) *Biochim. Biophys. Acta 1118*, 6−20.

Aguilar, C. F., Thomas, P. J., Moss, D. S., & Palmer, R. A. (1992) *J. Mol. Biol. 224*, 265−267.

Alber, T. W., Gilbert, W. A., Ponzi, D. R., & Petsko, G. A. (1973) *Ciba Found. Symp. 93*, 4−24.

Allen, K. N., Bellamacina, C. R., Ding, X., Jeffery, C. J., Mattos, C., Petsko, G. A., & Ringe, D. (1996) *J. Phys. Chem. 100*, 2605−2611.

Ball, J. A., Wilson, K. P., Zhang, X.-J., Farber, H. R., Nicholsoin, H., & Matthews, B. W. (1991) *Proteins: Struct., Funct., Genet. 10*, 10−21.

Baudet-Nessler, S., Jullien, M., Crosiom M. P., & Janin, J. (1993) *Biochemistry 32*, 8457−8464.

Bernstein, F. C., Koetzle, T. F., Williams, G. J. B., Meyer, E. F., Brice, M. D., Rogers, J. R., Kennard, O., Shimanouchi, T., & Tasumi, M. (1977) *J. Mol. Biol. 112*, 535−542.

Bientema, J. J., Schuller, C., Irie, M., & Carsana, A. (1988) *Prog. Biophys. Mol. Biol. 51*, 165−192.

Blackburn, P., & Moore, S. (1982) *Enzymes 15*, 317−433.

Bode, W., & Huber, R. (1978) *FEBS Lett. 90*, 265−269.

Bolen, D. W., Flogel, M., & Biltonen, R. (1971) *Biochemistry 10*, 4136−4140.

Borah, B., Chen, C. W., Egan, W., Miller, M., Wlodawer, A., & Cohen, J. S. (1985) *Biochemistry 24*, 2058−2067.

Borkakoti, N. (1983) *Eur. J. Biochem. 132*, 89−94.

Borkakoti, N., Moss, D. S., & Palmer, R. A. (1992) *Acta Crystallogr. B38*, 2210−2217.

Brooks, B. R., Bruccoleri, R. E., Olafson, B. D., States, D. J., Swaminathan, S. & Karplus, M. (1983) *J. Comput. Chem. 4*,187−217.

Brünger, A. T. (1992) *X-PLOR Version 3.0 Manual: a System for Crystallography and NMR*, Yale University, New Haven, CT.

Brünger, A. T., Kuriyan, J., & Karplus, M. (1987) *Science 223*, 458−460.

Campbell, R. L., & Petsko, G. A. (1987) *Biochemistry 26*, 8579−8584.

Chakrabarti, P. (1990a) *Biochemistry 29*, 651−658.

Chakrabarti, P. (1990b) *Protein Eng. 4*, 49−56.

Chakrabarti, P. (1993) *J. Mol. Biol. 234*, 463−482.

Clore, G. M., Bax, A., Wingfield, P. T., & Gronenborn, A. M. (1990) *Biochemistry 29*, 5671−5676.

Crosio, M. P., Janin, J., & Jullien, M. (1994) *J. Mol. Biol. 228*, 243−245.

delCarayre, S. B., & Raines, R. T. (1994) *Biochemistry 33*, 6031−6037.

de Llorens, R., Arus, C., Pares, X., & Cuchillo, C. M. (1989) *Protein Eng. 2*, 417−429.

deMel, V. R., Martin, P. D., Doscher, M. S., & Edwards, B. F. P. (1992) *J. Biol. Chem. 267*, 247−256.

deMel, V. R., Doscher, M. S., Glinn, M. A., Martin, P. D., Ram, M. L., & Edwards, B. F. P. (1994) *Protein Sci. 3*, 39−50.

Dewan, J. C., Mikami, B., Hirose, M., & Sacchettini, J. C. (1993) *Biochemistry 32*, 11963−11968.

Finzel, B. C. (1987) *J. Appl. Crystallogr. 20*, 53−55.

Fitzpatrick, P. A., Steinmetz, A. C. U., Ringe, D., & Klibanov, A. M. (1993) *Proc. Natl. Acad. Sci. U.S.A. 90*, 8653−8657.

Fitzpatrick, P. A., Ringe, D., & Klibanov, A. M. (1994) *Biochem. Biophys. Res. Commun. 198*, 675−681.

Gallagher, W. H., & Croker, K. M. (1994) *Protein Sci. 3*, 1602−1604.

Gorenstein, D. G., & Wyrwicz, A. M. (1974) *Biochemistry 13*, 3828−3836.

Haffner, P. H., & Wang, J. H. (1973) *Biochemistry 12*, 1608−1618.

Hemmings, A. M. (1993) *Acta Crystallogr. D49*, 541−547.

Hendrickson, W. A. (1985) *Methods Enzymol. 115*, 252−270.

Irie, M. (1965) *J. Biochem. 57*, 355−362.

Irie, M., Watanabe, H., Ohgi, K., Tobe, M., Matsumura, G., Arata, Y., Hirose, T. & Inayama, S. (1984a) *J. Biochem. 95*, 751−759.

Irie, M., Mikami, F., Monma, K., Ohgi, K., Wtaabe, H., Yamaguchi, R., & Nagase, H. (1984b) *J. Biochem. 96*, 89−96.

Iwahashi, K., Nakamura, K., Mitsui, Y., Ohgi, K., & Irie, M. (1981) *J. Biochem. 90*, 1685−1690.

Jones, J. A. (1985) *Methods Enzymol. 115*, 157−171.

Joseph-McCarthy, D., Fedorov, A. A., & Almo, S. C. (1996) *Protein Eng. 9*, 773−780.

Kabsch, W. (1988) *J. Appl. Crystallogr. 21*, 916−924.

Kartha, G., Bello, J., & Harker, D. (1967) *Nature (London) 213*, 862−865.

Katoh, H., Yoshinaga, M., Yanagita, T., Ohgi, K., Irie, M., Beintema, J. J., & Meinsma, D. (1986) *Biochim. Biophys. Acta 873*, 367−371.

Kim, E. E., Varadarajan, R., Wyckoff, H. W., & Richards, F. M. (1992) *Biochemistry 31*, 12304−12314.

Kurachi, K., Davie, E. W., Strydom, D. J., Riordan, J. F., & Vallee, B. L. (1985) *Biochemistry 24*, 5494−5499.

Laity, J. H., Shimotakahara, S., & Scheraga, H. A. (1993) *Proc. Natl. Acad. Sci. U.S.A. 90*, 615−619.

Lee, F. S., & Vallee, B. L. (1989) *Biochem. Biophys. Res. Commun. 161*, 121−126.

Li, J. R. T., & Walz, G. F. (1974) *Arch. Biochem. Biophys. 161*, 227−233.

Lisgrarten, J. N., Gupta, V., Maes, D., Wyns, L., Zegers, I., Palmer, R. A., Dealwis, L. G., Aguilar, C. F., Matthew, J. B., & Richards, I. M. (1982) *Biochemistry 21*, 4989−4999.

Luzzati, V. (1952) *Acta Crystallogr. 5*, 802−810.

Martin, P. D., Doscher, M. S., & Edwards, B. F. P. (1987) *J. Biol. Chem. 262*, 15930−15938.

Mazzarella, L., Capasso, S., Demasi, D., Di Lorenzo, G., Mattia, C. A., & Zagari, A. (1993) *Acta Crystallogr. D49*, 389−402.

Meadows, G. H., Roberts, G. C. K., & Jardetsky, O. (1969) *J. Mol. Biol. 45*, 491.

Miranker, A., & Karplus, M. (1991) *Proteins 11*, 29−34.

Mitsui, Y., Urata, Y., Torii, K., & Irie, M. (1978) *Biochim. Biophys. Acta 535*, 299−308.

Moroianu, J., & Riordan, J. F. (1994) *Biochem. Biophys. Res. Commun. 203*, 1765−1772.

Moult, J., Yaonath, A., Traub, W., Smilansky, A., Podajrny, A., Rabinovich, D., & Saya, A. (1976) *J. Mol. Biol. 100*, 179−195.

Nachman, J., Miller, M., Gilliland, G. L., Carty, R. P., Pincus, M., & Wlodawer, A. (1990) *Biochemistry 29*, 928−937.

Nicholls, A., Sharp, K A., & Honig, B. H. (1991) *Proteins 11*, 281−296.

Pares, X., de Lorens, R., Arus, C., & Cuchillo, C. M. (1980) *Eur. J. Biochem. 105*, 571−579.

Pavlosky, A. G., Borisova, S. N., Borisov, V. V., Antonov, I. V., & Karpeisky, M. Y. (1978) *FEBS Lett. 92*, 258−262.

Potts, J. T., Berger, A., Cooke, J., & Anfinsen, C. B. (1962) *J. Biol. Chem. 237*, 1851−1855.

Richards, F. M., & Wyckoff, H. W. (1971) *Enzymes (3rd Ed.) 4*, 647−806.

Richardson, R. M., Pares, X., & Cuchillo, C. M. (1990) *Biochem. J. 267*, 593−599.

Rossmann, M. G., & Argos, P. (1975) *J. Biol. Chem. 250*, 7525.

Roussel, A., & Cambillau, C. (1989) in *Silicon Graphics Geometry Partner Directory* (Silicon Graphics, Ed.) pp 77−78, Silicon Graphics, Mountain View, CA.

Ruterjans, H., & Witzel, H. (1969) *Eur. J. Biochem. 9*, 118−127.

Sanishvilli, R., Volz, K. W., Westbrook, E. M., & Margoliash, E. (1995) *Structure 3*, 707−716.

Sawada, F., & Irie, M. (1969) *J. Biochem. 66*, 415−418.

Sheriff, S. (1987) *J. Appl. Crystallogr. 20*, 55−57.

Smyth, D. G., Stein, W. H., & Moore, S. (1963) *J. Biol. Chem. 238*, 277−234.

Strydom, D. J., Fett, J. W., Lobb, R. R., Alderman, E. M., Bethune, J. L., Riordan, J. F., & Vallee, B. L. (1985) *Biochemistry 24*, 5486−5494.

Tarragona-Fiol, A., Eggelte, H. J., Harbron, S., Sanchez, C. J., Ward, J. M., & Rabin, B. R. (1993) *Protein Eng. 6*, 901−906.

Usher, D. A., Richardson, D. I., & Eckstein, F. (1970) *Nature (London) 288*, 663.

Usher, D. A., Erenrich, E. S., & Eckstein, F. (1972) *Proc. Natl. Acad. Sci. U.S.A. 69*, 115.

Varadarajan, R., & Richards, F. M. (1992) *Biochemistry 31*, 315−327.
Williams, R. L., Greene, S. M., & McPherson, A. (1987) *J. Biol. Chem. 262*, 16020−16030.
Witzel, H. (1963) *Prog. Nucleic Acid Res. 2*, 221−251.
Wlodawer, A. (1985) in *Biological Micromolecules and Assemblies*, Vol. 2, pp 393−439, John Willey and Sons, New York.
Wlodawer, A., & Hodgson, K. O. (1975) *Proc. Natl. Acad. Sci. U.S.A. 72*, 398−399.
Wlodawer, A., Deisenhofer, J., & Huber, R. (1987a) *J. Mol. Biol. 193*, 145−156.
Wlodawer, A., Nachman, J., Gilliland, G. L., Gallagher, W., & Woodward, C. (1987b) *J. Mol. Biol. 198*, 469−480.
Wlodawer, A., Svensson, L. A., Sjolin, L., & Gilliland, G. (1988) *Biochemistry 27*, 2705−2717.
Wodak, S. Y., Liu, M. Y., & Wyckoff, H. W. (1977) *J. Mol. Biol. 116*, 855−875.
Wyckoff, H. W., Carlson, W., & Wodak, S. (1977) in *Nucleic Acid−Protein Recognition* (Vogel, N. J., Ed.) pp 569−500, Academic Press, New York.

BI961533G